HHS Public Access

Author manuscript

Nat Biotechnol. Author manuscript; available in PMC 2020 February 02.

Published in final edited form as:

Nat Biotechnol. 2019 August ; 37(8): 895–906. doi:10.1038/s41587-019-0197-9.

Epicardial cells derived from human embryonic stem cells augment cardiomyocyte-driven heart regeneration

Johannes Bargehr[1,2], **Lay Ping Ong**[1,2], **Maria Colzani**[1,2], **Hongorzul Davaapil**[1,2], **Peter Hofsteen**[3], **Shiv Bhandari**[3], **Laure Gambardella**[1,2], **Nicolas Le Novère**[4], **Dharini Iyer**[1,2], **Fotios Sampaziotis**[1], **Florian Weinberger**[3], **Alessandro Bertero**[3], **Andrea Leonard**[3], **William G Bernard**[1,2], **Amy Martinson**[3], **Nichola Figg**[2], **Michael Regnier**[5], **Martin R Bennett**[2], **Charles E Murry**[3,5,6,Ω], **Sanjay Sinha**[1,2,Ω]

[1]The Anne McLaren Laboratory, Wellcome Trust –MRC Cambridge Stem Cell Institute, Forvie Site, University of Cambridge, Robinson Way, Cambridge CB2 0SZ, UK

[2]Division of Cardiovascular Medicine, University of Cambridge, ACCI Level 6, Box 110, Addenbrooke's Hospital, Hills Road, Cambridge CB2 0QQ, UK

[3]Department of Pathology, Center for Cardiovascular Biology, Institute for Stem Cell and Regenerative Medicine, University of Washington, Seattle, WA, US

[4]Babraham Institute, Babraham Hall, Babraham CB22 3AT, UK

[5]Department of Bioengineering, University of Washington, Seattle, WA, US

[6]Department of Medicine/Cardiology, University of Washington, Seattle, WA, US

Abstract

The epicardium and its derivatives provide trophic and structural support for the developing and adult heart. Here we tested the ability of human embryonic stem cell (hESC)-derived epicardium to augment the structure and function of engineered heart tissue (EHT) *in vitro* and to improve efficacy of hESC-cardiomyocyte grafts in infarcted athymic rat hearts. Epicardial cells markedly

Corresponding Authors: Dr. Sanjay Sinha, The Anne McLaren Laboratory, WT-MRC Cambridge Stem Cell Institute, West Forvie Building, Forvie Site, University of Cambridge, Robinson Way, CB2 0SZ Cambridge, UK, Tel.: +44 1223 747479, Fax: +44 1223 763350., ss661@cam.ac.uk, Dr. Charles E. Murry, Institute for Stem Cell and Regenerative Medicine, University of Washington, 850 Republican Street, Brotman Building Room 453, Seattle, WA 98109, USA, Tel: +1-206-616-8685, Fax: +1-206-897-1540, murry@uw.edu.

ΩEqual Contributions

Author contributions: JB: Principal experimentalist, study design and conceptualisation, data acquisition and interpretation, production of figures, manuscript writing; LPO: tissue culture, 3D-EHT generation, force measurement, assistance during surgery; MC: tissue culture, 3D-EHT generation; HD: force measurement and QRT-PCR; PH: preparation of cell suspension on the day of transplantation, necropsy, assistance during surgery, postoperative animal care; SB: casting of 3D-EHT, force measurement; LG: tissue histology, immunofluorescence, sample preparation for RNAseq; NLN: bioinformatics analysis; DI: conceptual ideas, critical revision of the manuscript for important intellectual content; FS: Critical revision of the manuscript for important intellectual content; FW: functional analysis of echocardiographs; AB: gene expression analysis; AL: experimental guidance and force measurement data analysis; WGB: data interpretation and logistics; AM: animal surgery and logistics; NF: processing of histologic tissue, preparation of slides; MR: force measurement equipment; MRB: critical revision of the manuscript for important intellectual content; CEM: design and concept of the study, obtaining research funding, study supervision, editing and final approval of the manuscript; SS: design and concept of the study, obtaining research funding, study supervision, interpretation of data, editing and final approval of the manuscript.

Data availability:

The raw data that support the findings of this study are available from the corresponding author upon reasonable request.

enhanced the contractility, myofibril structure and calcium handling of human EHTs, while reducing passive stiffness compared to mesenchymal stromal cells. Transplanted epicardial cells formed persistent fibroblast grafts in infarcted hearts. Co-transplantation of hESC-derived epicardial cells and cardiomyocytes doubled graft cardiomyocyte proliferation rates *in vivo,* resulting in 2.6-fold greater cardiac graft size and simultaneously augmenting graft and host vascularization. Notably, co-transplantation improved systolic function compared with hearts receiving either cardiomyocytes alone, epicardial cells alone or vehicle. The ability of epicardial cells to enhance cardiac graft size and function make them a promising adjuvant therapeutic for cardiac repair.

Keywords

Epicardium; epicardial; cardiac regeneration; regenerative medicine; human embryonic stem cells; myocardial infarction; cell transplantation; embryonic origin

Introduction

Despite major advances in the treatment of heart failure due to systolic impairment, therapeutic approaches have fallen short of addressing the cause of the problem; injury of the mammalian heart leads to irreversible loss of contractile myocardial tissue which is incapable of regeneration. At the turn of the millennium heart failure was widely identified as an emerging epidemic[1]. To date 5.6 million patients in the US alone and 23 million worldwide are suffering from heart failure with 50% dying within 5 years after being diagnosed[2, 3]. Current treatment is limited to ameliorating symptoms and slowing the natural progression of the disease but fails to compensate for the loss of contractile myocardium post-injury.

Regenerative medicine may hold the key to effectively treating heart failure by using stem cell-derived cardiovascular cells and tissues to restore full contractile function[4, 5]. Of all stem cell types, human pluripotent stem cells such as embryonic stem cells (hESC) and induced pluripotent stem cells (hiPSC) have the greatest potential for forming cardiovascular tissues, reliably giving rise to cardiomyocytes[6–8], endothelial cells[9, 10], smooth muscle cells[11] and more recently also epicardial and endocardial-like cells[12–15] under chemically defined conditions. Furthermore, hESC-derived cardiomyocytes have been successfully used to remuscularize infarcted rat [8] and guinea pig[16, 17] hearts, resulting in electrical integration and preserving cardiac function. The clinical potential of this technology has also been demonstrated in non-human primate models, where transplantation of human or monkey pluripotent stem cell (PSC)-derived cardiomyocytes resulted in substantial remuscularization of the infarcted heart and restoration of cardiac function[18–20].

While mammalian heart regeneration has made progress, hurdles remain, such as relative immaturity of transplanted cells, suboptimal graft retention, insufficient cellular proliferation and a small graft size. *In vitro*, hPSC-derived cardiomyocytes derived from most protocols at best resemble cardiomyocytes found in a first trimester fetus, which may limit the functional benefits post-transplantation[21]. To date, little attention has been devoted to a supportive cell

type that would promote maturity of hESC-derived cardiomyocytes and increase the graft size post-transplantation *in vivo*.

In early mammalian heart development, the epicardium plays a pivotal role as a progenitor cell source and provides trophic support for developing cardiomyocytes. Because the epicardium gives rise to cardiac fibroblasts and coronary smooth muscle cells, it is essential for the formation of a functioning connective tissue and coronary vasculature[22, 23]. Moreover, epicardium-derived cells are essential for cardiac proliferation and compaction[24–26] and have been reported to promote cardiomyocyte maturation[27–29]. Given its trophic role in heart development we hypothesized that epicardial cells could promote cardiomyocyte maturation and contractility in hESC-based 3D-engineered heart tissues (EHTs) *in vitro* and enhance engraftment and maturity leading to potential functional benefits when co-transplanted with hESC-derived cardiomyocytes *in vivo*.

We report here that hESC-derived epicardium promotes the development of 3D-EHTs *in vitro* and cardiac grafts *in vivo* via cardiomyocyte maturation, proliferation and contraction. In the infarcted heart, hESC-derived epicardial cells (hESC-EPI) also increase endogenous neo-vessel development and enhance hESC-CM proliferation and subsequent maturation, thus creating larger grafts of human myocardium that further enhance ventricular function. By recapitulating key developmental steps, the epicardium augmented cardiomyocyte function, making it a promising adjuvant therapy in regenerative medicine.

Results

HESC-derived epicardial cells promote cardiomyocyte maturation in 3D-EHT

We first generated hESC-derived GFP-transgenic epicardial cells and wild-type (WT) cardiomyocytes as previously described[8, 12], (Fig. 1a–b). Epicardial cells expressed epicardial and epithelial markers, WT1 and pan-cytokeratin, but no mesenchymal markers such as vimentin after their derivation *in vitro*[12, 30]. The functionality of epicardial cells was initially demonstrated through differentiating them to cardiac fibroblasts *in vitro* under chemically defined conditions that included VEGF and FGF. At the end of this differentiation protocol they expressed the fibroblast and mesenchymal markers, S100A4, DDR2 and vimentin, but lost their epithelial character indicating successful epithelial to mesenchymal transition (EMT). During epicardial to fibroblast differentiation, WT1 was downregulated while the fibroblast marker S100A4 was gradually upregulated. (Supplementary Fig. 1a–e).

Next, we tested the utility of epicardial cells in the context of 3D engineered heart tissues (EHTs). We incorporated epicardial cells along with hESC-CMs into collagen-based 3D-EHTs[31], which developed for 14 days under passive stress before they were subjected to histological and functional assessment (Fig. 1c–d). To investigate the potency of epicardial cells in 3D-EHT we compared them with constructs containing: (1) cardiomyocytes alone; (2) cardiomyocytes and hESC-derived mesenchymal cells; (3) cardiomyocytes and primary human mesenchymal stromal cells (MSCs) from bone marrow. Both epicardial cells as well as primary mesenchymal cells had the strongest effects on tissue remodelling and

compaction whereas tissues containing high-purity cardiomyocytes alone demonstrated minimal compaction (Fig. 1e–g).

Whilst in the tissues, hESC-EPI underwent EMT as indicated by the increase in expression of vimentin and decrease in pan-cytokeratin comparing constructs after 7 days and 14 days of their development. In this context, epicardial derivates have previously been termed epicardium-derived cells (EPDCs)[23]. EPDCs are positive for Vimentin and S100A4, indicative of a fibroblast phenotype (Supplementary Fig. 2a–c).

To determine the state of cardiomyocyte maturity, histological sections of the 3D-EHTs were stained for sarcomeric proteins, and the sarcomere length, cell diameter, cell sectional area and myofibril alignment were quantified. HESC-EPI promoted the greatest sarcomere length, cell diameter, cell sectional area and myofibril alignment, which correlate with cardiomyocyte maturation, compared to primary MSCs, hESC-derived MSCs or CM alone (Fig. 1h–j, supplementary Fig. 3a). 3D-EHTs containing hESC-EPI and primary MSC exhibited the greatest degree of sarcomeric organisation (Supplementary Fig. 3b). Furthermore, constructs containing hESC-EPI expressed more connexin 43, a marker of electrical connectivity between cardiomyocytes, compared to the other groups (Supplementary Fig. 2d–e). Gene expression by qRT-PCR demonstrated trends consistent with increases in the ratios of adult/fetal isoforms of contractile proteins (*MYH7/MYH6*, *MYL2/MYL7* and *TNNI3/TNNI1)*, all indicators of cardiomyocyte maturity (Supplementary Fig. 4). In conclusion, hESC-derived epicardial cells replicate key steps of early embryonic heart development in 3D-EHTs resulting in increased cardiomyocyte maturation.

HESC-derived epicardial cells enhance functional maturation of 3D-EHT

We next tested whether the beneficial effects of hESC-derived epicardial cells observed histologically also translated to an increase in contractility. EHT constructs were transferred to a myograph with a length controller and a force transducer (Supplementary Fig. 5a); constructs containing CM and either hESC-MSC or primary MSC or hESC-EPI exhibited a Frank-Starling relationship, where twitch force increased linearly with increasing preload. In line with the histological finding that high-purity CM alone do not result in efficient tissue remodelling, cardiomyocyte maturation or electrical connectivity, we did not observe coordinated contraction or measurable force production in 3D-EHTs containing CM alone. Constructs containing hESC-EPI produced the greatest total force amongst the 4 groups. Additionally, EHTs containing hESC-EPI showed the greatest increase in active force production with increasing strain (i.e. the greatest contractility) compared to primary MSCs and hESC-MSCs (Fig. 2a, Supplementary Fig. 5b). At the same time, 3D-EHTs containing hESC-EPI produced the least passive force compared to primary MSCs or hESC-MSCs, which would correspond to a more compliant tissue with better relaxation potential during diastole (Fig. 2b).

When assessing the Ca^{2+}-handling of the constructs, those containing hESC-EPI and primary MSCs accounted for the most mature Ca^{2+} transients (Fig. 2c–d). Constructs containing EPDCs had more rapid Ca^{2+}-release and Ca^{2+}-decay compared to those with primary MSCs (Fig. 2e, Supplementary Fig. 5c–d). Constructs containing hESC-MSC

displayed irregular and broad Ca^{2+} transients, reflecting less coordinated beating. In those containing CM-only, no coordinated Ca^{2+} transients were detectable, but rather asynchronous contraction of single non-connected cardiomyocytes was observed, which translated to noise in multicellular regions of interest.

Next, we tested if the ability of epicardial cells to promote 3D-EHT function is independent of the parental hESC line. We generated EHTs where cardiomyocytes and EPDCs were differentiated from the same H9 line, as well as with cardiomyocytes from H9 cells and EPDCs from RUES2 hESCs. In both contexts, the EPDC-containing EHTs showed superior contractility and Ca^{2+} dynamics compared to EHTs made with hESC-MSCs or primary MSCs. These experiments demonstrated that enhancement of EHT function by EPDCs is a general attribute of epicardial cells and not a line-dependent artefact (Supplementary Fig. 6a–b, Supplementary Fig. 7a–d).

Furthermore, in a separate experiment we determined the nature of the non-cardiomyocyte population obtained upon differentiation of high-purity cardiomyocytes by flow cytometry using markers previously described[32]. We found positivity for THY1 and PDGFR-β and to a minor degree for CD31 and NKX2.5 in this cTnT-negative cell population (Supplementary Fig. 8). Overall, this demonstrated a mesenchymal and fibroblast-like nature to these non-cardiomyocytes and was comparable between RUES2- and H9-derived cells.

In conclusion, hESC-derived epicardial cells promote functional maturation of 3D-EHT. These findings encouraged us to explore their use *in vivo* as an adjunct to cardiomyocyte transplantation for cardiac repair.

Epicardial cells engraft and differentiate in the myocardial infarct

To assess the response of hESC-derived epicardial cells to engraftment *in vivo* we performed a series of pilot transplants into the infarct zone of athymic rats (Supplementary Fig. 9a). Because most non-myocytes that are transplanted into the heart rapidly die[33], we subjected the epicardial cells to heat shock and a prosurvival cocktail (PSC) of anti-apoptotic and anti-necrotic factors. At 7 days post-transplantation we found small grafts in 3 out of 4 animals receiving 2×10^6 cells and larger grafts in all 4 animals receiving 4×10^6 cells (Supplementary Fig. 9b–c). To maximise survival at 28 days post-transplantation, we delivered 6×10^6 cells and found large grafts in 6 out of 6 animals (Supplementary Fig. 9d), indicating the grafts survive long term. We confirmed in a separate experiment that delivery with heat shock + PSC is required for engraftment of epicardial cells (Supplementary Fig. 10a–c). Conversely, epicardial cell transplantation in NOD scid gamma mice, without heat shock + PSC, demonstrated no detectable graft formation at 28 days (Supplementary Fig. 11a–c).

At 7 days post-transplantation the EPDCs co-expressed pan-cytokeratin and vimentin, indicating ongoing EMT. At 28 days post transplantation EMT was essentially complete, with all grafted cells expressing vimentin and almost no detectable expression of pan-cytokeratin (Supplementary Fig. 9e–f). A small subpopulation of grafted vimentin-positive cells co-expressed WT1 on day 7 and day 28. This reflects the human fetal heart, where activated vimentin+ epicardial cells invade the compact myocardium with a subpopulation retaining WT1 expression (Supplementary Fig. 9g–g‘). At 28 days the grafted epicardial

cells expressed S100A4, suggesting a fibroblast phenotype, whereas they neither expressed SM22α nor integrated into blood vessel walls, (Supplementary Fig. 12a–b). Grafted cells were negative for the cardiac marker α-actinin and the endothelial marker human Lectin (Supplementary Fig. 12c–e). Taken together, these data indicate that EPDCs differentiate into cardiac fibroblast-like cells with no formation of cardiomyocytes, endothelial cells or smooth muscle cells.

Because EPDCs readily form smooth muscle cells *in vitro,* we hypothesized that the infarct environment inhibited this differentiation pathway. To test this, we delivered hESC-EPI in PSC onto the chorionic vasculature of chick embryos. After 5 days the human EPDCs had integrated into the walls of host vessels and expressed SM22α (Supplementary Fig. 13a–c). Thus, the epicardial cells are multipotent and in an embryonic environment readily differentiate into vascular smooth muscle, whereas in the adult infarct they form fibroblast-like cells.

Co-transplantation of epicardial cells and cardiomyocytes augments microvascular density

The long-term persistence of hESC-derived epicardial cells in infarcted hearts led us to hypothesize that these cells would exhibit a trophic effect on grafted hESC-cardiomyocytes and the host myocardium. To test this, we performed a co-transplantation study where four groups of athymic rats either received an injection of 5×10^6 hESC-derived epicardial cells (EPI), 10×10^6 hESC-derived cardiomyocytes (CM), the combination of both (EPI+CM: 5×10^6 hESC-derived epicardial cells plus 10×10^6 cardiomyocytes) or vehicle control (PSC; Fig. 3a). Four weeks post transplantation no difference in infarct size was found between the groups, ruling out effects on infarct scar healing (Fig. 3b–c).

To assess whether cell transplantation had an effect on host vessel recruitment, we quantified the microvascular density in the cardiac grafts, the infarct zone and the non-injured border zone (Fig. 3d). Microvascular density was significantly increased in cardiac grafts of animals that were co-transplanted with epicardial cells and cardiomyocytes. Furthermore, erythrocytes were readily detectable in the lumens of the vessels, indicating perfusion via the coronary circulation (Fig. 3e, Supplementary Fig. 14a). We also observed an increase in microvascular recruitment in the infarct zone and in the non-injured border zone of the infarct, which was highest in EPI+CM, followed by CM, then EPI and finally vehicle control (Fig. 3f–g). To assess the timing of microvascular sprouting we made use of our pilot trial dataset and demonstrated that, epicardial cells alone lead to a significant increase in microvascular density in the infarct- and borderzone by day 28 but not by day 7 post transplantation, indicating delayed angiogenic effects (Supplementary Fig. 14b–e).

To address the maturity of neo-vessels we also screened the three areas of interest for presence of smooth muscle cell coated arteries. Vessels containing SM22α+ mural cells were abundant in the infarct zone and the border zone of all groups. However, when assessing their presence within cardiac grafts we observed smooth muscle cell coated vessels in the EPI+CM group but not in the CM-alone group, suggesting epicardial cells promote smooth muscle encoatment and vascular maturation within the graft (Supplementary Fig. 14f–k). Absence of co-staining for SM22α and human mitochondria further confirmed that the smooth muscle coats were rat-derived, and that epicardial cells were also not able to

differentiate to smooth muscle cells in the infarct zone in the presence of cardiomyocytes (Supplementary Fig. 14l). In summary, hESC-derived epicardial cells create a more highly vascularized cardiac graft, and microvascular density surrounding scar and border zone, which should promote a more favourable niche for hESC-cardiomyocyte engraftment and function.

Co-transplantation promotes cardiac graft size, proliferation and maturity

We next assessed the effects of epicardial cells on the cardiac grafts. Given the trophic effects of epicardial cells on cardiomyocytes *in vitro* we first investigated whether co-transplantation would affect cardiac graft size. Cardiac grafts were readily identified with antibodies directed against β-MHC (MYH7; whereas rat cardiomyocytes predominantly express α-MHC/MHY6) and co-expressed α-actinin. Cardiac grafts were 2.6-fold larger when cardiomyocytes were co-transplanted with epicardial cells, compared to cardiomyocytes alone, averaging 3.9±1.6% of the left ventricle vs 1.5±0.9% of the left ventricle, respectively (Fig. 4a–b; Supplementary Fig. 14m).

Because epicardial cells secrete growth factors for cardiomyocytes during development, we hypothesized that epicardial cells augmented graft size via increased cardiomyocyte proliferation. All rats in this phase of the study were pulsed with the thymidine analogue, BrdU, on 1, 3, 7 and 14 days post-cell delivery. To determine cumulative proliferation rates in the grafts we stained with antibodies directed against BrdU and the human-specific cardiac marker β-MHC. The proliferative index of β-MHC positive cells was 2-fold higher in animals that received the combination of hESC-EPI and cardiomyocytes (8%±1.4%) compared with cardiomyocytes alone (4±0.9%, $p<0.0001$; Fig. 4c–d). Conversely, there was no difference in the proliferative index of vimentin-positive EPDCs in animals receiving epicardial cells alone or epicardial cells with cardiomyocytes (Supplementary Fig.15a–b). Taking the graft cardiomyocyte BrdU rates as daily averages of DNA synthesis, and assuming that the cell cycle lasts 24 hours, hESC-CM graft expansion can be calculated for each group. For 28-day grafts, control expansion would be 1.04^28, or 3.0-fold expansion, while in co-transplantation studies it would be 1.08^28, or 8.6-fold expansion. This predicts a 2.9-fold difference in graft size, which is quite close to our observed 2.6-fold difference. Thus, although we cannot rule out a role for increased graft survival, these data indicate that enhanced cardiomyocyte proliferation is a major driver for the increased cardiomyocyte graft size observed with hESC-derived epicardial cell co-transplantation.

Given the epicardial effects on cardiomyocyte maturation *in vitro,* we assessed the sarcomere length of the cardiac grafts. In line with our findings *in vitro,* cardiomyocytes that were co-transplanted with epicardial cells exhibited a greater sarcomeric length and cell diameter as well as a 77% larger cell sectional area (Fig. 4f–h) than those that were transplanted alone, indicative of a more mature phenotype. Additionally, we demonstrated that co-transplantation of cardiomyocytes with epicardial cells leads to an isoform switch from ssTnI to cTnI in cardiac grafts (Fig. 4e).

As cardiac fibrosis impedes structural integration of grafts and host[34], we were concerned that epicardial cell-derived fibroblasts might interfere with gap junctions between graft and host cardiomyocytes. To investigate this, we performed combined immunostaining for β-

MHC, cTnT and the gap junction protein connexin43. Gap junctions between graft and host were seen in multiple areas across all animals, demonstrated by connexin43 expression between neighbouring human and rat cardiomyocytes (Fig. 4i). While, epicardial cells themselves can express connexin43[35, 36], the gap junctions identified in our study were predominantly between cardiomyocytes. In conclusion, hESC-derived epicardial cells promote cardiac graft size, in part through proliferation, and they enhance maturation/myofibril development, while still permitting structural integration of grafted cardiomyocytes with the recipient myocardium.

Co-transplantation promotes cardiac function

To assess the functional effects of cardiac grafts on global host heart function, we performed cardiac ultrasound on all animals prior to infarction, immediately before cell injection and after 28 days of follow-up. The ultrasound scans (AM) and their interpretations (JB and FW) were performed by investigators who were blinded to the treatment to prevent bias. All groups exhibited comparable left ventricular (LV) dilation and decline in LV function after infarction, consistent with the histological finding of comparable infarct sizes (Fig. 5a–c; supplementary table 1). Compared with their pre-injection (post-infarction) baseline values, the vehicle control group displayed a 9±5.4% decline in fractional shortening by 4 weeks after injection, indicating a progression towards heart failure ($p<0.0001$ vs. baseline). The EPI group showed a 5.3±6.5% decline in fractional shortening. Similar to previous reports from our group[8], transplantation of cardiomyocytes-only preserved cardiac function over the 4-week period, indicating that CM transplantation prevented the progression to heart failure. Importantly, animals receiving combined CM+EPI grafts showed a 4.5±3.6% improvement in fractional shortening, indicating that co-transplantation significantly improved LV function ($p=0.0175$ vs. cardiomyocytes-only). Furthermore, we demonstrated that in the CM and CM+EPI groups, improvements in LV function correlate linearly with graft size (Supplementary Fig. 15c).

Comparing pre- and post-injection values, left-ventricular end-systolic dimension (LVESD) remained stable in the CM+EPI group and increased in the CM only group, followed by greater increases in the EPI and the vehicle control group. The change in LVESD in the CM +EPI group was significantly smaller than in the vehicle control group but the difference to the CM only group or the EPI group did not reach statistical significance (Fig. 5d–e). For left ventricular end diastolic dimension (LVEDD), ANOVA did not yield a significant difference (Fig. 5f–g). Taken together, these studies show that co-transplantation of hESC-derived epicardial cells with cardiomyocytes leads to a greater increase in cardiac function compared to transplantation of cardiomyocytes alone. Furthermore, this benefit manifests principally as enhanced systolic function rather than impacting left ventricular remodelling.

To investigate whether these effects would be present in the long term, we followed a subset of 4–5 animals per group for up for 3 months. Three months after cell grafting hESC-EPI as well as hESC-derived cardiomyocytes were still present in the infarct zone as confirmed by anti-human mitochondrial staining (Supplementary Fig. 16a–c). In line with the 28-day follow-up, at 84 days post transplantation no differences were found in infarct size between the four study groups (Supplementary Fig. 16d). Functional analysis demonstrated long-term

perpetuation of benefits perceived at 1 month due to persistent systolic improvement. Fractional shortening showed no decline in animals receiving CM+EPI or CM-only but a significant decline in animals receiving either EPI or vehicle control. While there was no difference in the change of fractional shortening between day 28 and day 84 among the groups, the change occurring between day 4 and day 84 was significantly greater in the CM +EPI group compared to CM only or EPI only or vehicle control (Supplementary Fig. 16e–f). Indeed the 4.5% improvement in FS of epicardial cell co-therapy over cardiomyocytes alone seen at 4 weeks increased further to 9.6% by 12 weeks (Supplementary Fig. 16f). To summarise, hESC-derived cellular grafts and related functional improvement in cardiac function persist in the long term.

RNA-sequencing reveals the epicardial secretome

Finally, to address the question of putative mediators of epicardial cell-driven cardiac repair we performed RNA sequencing of hESC-derived epicardium as used for all *in vitro* and *in vivo* experiments. In embryonic heart development, the neural crest (NC) is essential for pharyngeal arch organisation and outflow tract septation but lineage tracing studies have to date not suggested a role in cardiac maturation[37–39]. We first used hESC-derived NC cells in 3D-EHTs, demonstrating the inability of this cell population to result in structural and functional heart maturation, in contrast to epicardial cells (Supplementary Fig. 17a–b). We therefore used NC cells as a negative control for RNA-sequencing (Fig. 6a, Supplementary table 2).

As epicardial cells resulted in stark effects on tissue remodelling of 3D-EHTs and because it has been demonstrated that the extracellular matrix plays a key role in epicardial-driven heart repair, we focused on extracellular matrix molecules secreted by epicardial cells and differentially expressed in the hESC-derived NC cells (Supplementary table 2). The heatmap shown in Figure 6a displays differentially expressed genes with an adjusted p-value $<1\times10^{-7}$ (a complete list of the genes and their expression is shown in supplementary table 2). Amongst them, Fibronectin is one of the most differentially expressed candidates. We then performed a gene ontology (GO) enrichment analysis, which further highlights a potential role for ECM expressed by hESC-EPI in myocardial development and maturation (Fig. 6b–c, Supplementary Fig. 18).

We first demonstrated that Fibronectin was also abundantly expressed at the protein level in 3D-EHT containing epicardial cells but to a lesser degree in constructs containing hESC-MSC, primary MSC or cardiomyocytes alone (Fig. 6d). Furthermore, Fibronectin was highly expressed in cardiac grafts *in vivo* in animals receiving epicardial cells and cardiomyocytes or epicardial cells alone but only at a rudimentary level in those receiving cardiomyocytes alone or vehicle control (Fig. 6e). In summary, RNA-sequencing has provided the secretome of hESC-derived epicardium and identified a potential involvement of extracellular matrix remodelling in the process of cardiac maturation in vitro and in vivo. These data provide a valuable target library for future cardiac repair strategies.

Discussion

This study was designed to address two gaps in knowledge: the immaturity of hPSC-derived cardiomyocytes, and the inefficient remuscularization of infarcts following hPSC-CM transplantation. Because of the key trophic role played by the epicardium during development, we hypothesized that hPSC-epicardial cells would promote cardiomyocyte proliferation and maturation, resulting in better EHT formation *in vitro* and better infarct remuscularization *in vivo.* We found that hESC-derived epicardial cells undergo EMT to fibroblast-like cells both *in vitro* and *in vivo*. In EHTs EPDCs augment tissue structure and function, resulting in increased cardiomyocyte size, sarcomere length, force production and augmented Ca^{2+} handling. When co-delivered with hESC-CMs into myocardial infarcts, EPDCs stimulate hESC-CM proliferation, increasing remuscularization by 2.6-fold. Additionally, EPDCs stimulate vascularization within the graft, infarct scar and in the borderzone host myocardium. These changes are accompanied by remodelling of the ECM, including high levels of fibronectin deposition. Finally, co-delivery of hESC-derived epicardium with hESC-CM results in significantly improved ventricular function post-infarction.

The pivotal role of the epicardium in heart development is well recognized. During early embryonic heart formation the epicardial tissue gives rise to coronary smooth muscle cells[22, 23] and myocardial fibroblasts[24, 25, 40]. While smooth muscle cells are critical for formation of the coronary vasculature, cardiac fibroblasts are essential for myocardial proliferation and compaction[26]. Conversely, inhibiting proepicardial outgrowth results in pathologic formation of the coronary vessels and non-compaction cardiomyopathy[41]. The trophic effect of quail and rat epicardium-derived cells has been demonstrated in co-culture experiments resulting in structural and functional maturation of cardiomyocytes[27, 29]. Our data show that co-culture of hESC-derived epicardial cells and cardiomyocytes results in compaction and structural as well as functional maturation of 3D-EHT. More specifically we demonstrate that hESC-derived epicardium outcompetes both hESC-derived MSCs as well as primary MSCs in terms of force generation and Ca^{2+}-handling, corroborating the functional role of its embryonic identity. The functional potency of epicardial cells might prove broadly applicable to current tissue engineering strategies, that would benefit from enhanced structural integrity and function of cardiomyocytes[42].

In neonatal mice and in zebrafish, the epicardium is thought to have a key role in facilitating myocardial regeneration following injury[43, 44]; in contrast the adult mammalian heart displays inadequate epicardial activation and fails to regenerate myocardium post-injury. In this context it has been demonstrated that embryonic cardiac fibroblasts induce greater cardiac proliferation than their adult counterparts[26]. Consequently, we propose that the fetal-stage epicardium generated by hESCs may preferentially promote regeneration.

It is important to consider the mechanism of action through which the epicardial cells improve the impact of cardiomyocyte transplantation. Since cardiomyocytes are already effective by themselves, the 2.6-fold enhancement of cardiomyocyte engraftment induced by epicardial cell co-delivery may underlie much of the benefit on cardiac function. The positive correlation of cardiac graft size and delta FS (%) corroborates this interpretation

(Supplementary Fig.15c). Most of this increase in engraftment can be accounted for by the 2-fold increase in cardiomyocyte DNA synthesis rates induced by epicardial cell co-delivery, although beneficial effects on cardiomyocyte survival cannot be ruled out. Another important factor, however, is that the EPDCs induced a significant amount of angiogenesis in the graft, infarct scar and boderzone host myocardium. Increased vascularization should improve the function of both graft and host tissues and could contribute to the beneficial effect.

A third potential mechanism was raised by our RNA-seq studies, which demonstrated that hESC-derived epicardial cells synthesize an embryonic ECM that is particularly rich in fibronectin. It has been demonstrated that the secretion of fibronectin by epicardial cells is required for heart regeneration in zebrafish[45]. In line with these findings it was demonstrated that the orchestrated secretion of fibronectin, collagen and heparin-binding EGF-like growth factor by embryonic but not adult fibroblasts resulted in cardiomyocyte proliferation[26]. We therefore propose that the matrix laid down by hESC-derived epicardial cells is likely to exhibit developmental cues that are absent in mature post-infarct myocardium, providing an advantageous niche in a hostile environment and the GO analyses of RNA sequencing data are in support of this. Further elucidation of the observed crosstalk between epicardium and cardiomyocytes might aid ongoing tissue engineering and cell therapy endeavours and the extensive data on epicardially-expressed genes made available here provides a rich resource for further study. These mechanisms are not mutually exclusive and could co-exist.

Finally, although we favour the notion that the salutary effects of co-delivering cardiomyocytes plus epicardial cells results from the impact on cardiomyocyte graft size, vascularization and ECM, we cannot rule out a paracrine effect from simply increasing the number of delivered cells in the combined cell group. Indeed, our data do not permit distinguishing the direct mechanical effects of the cardiomyocyte grafts from the paracrine factors they secrete; presumably both mechanisms may co-exist and be augmented by larger cardiomyocyte grafts. However, this does not detract from our primary conclusion that hESC-derived epicardial cells recapitulate their embryonic role in the post-MI setting by promoting hESC-derived cardiomyocyte proliferation and maturity and at the same time favourably influencing host tissue regeneration.

Two other pioneering studies have demonstrated that human primary epicardial cells improve function of the infarcted heart and that co-transplantation of adult cardiovascular progenitors with epicardial cells exerts a synergistic effect that exceeds that of monotherapy[33, 46]. There were several important differences with our study, including their use of epicardial cells and cardiac progenitor cells derived from the adult human heart (vs. our use of hESC derivatives) and their use of NOD-SCID mice with permanent coronary ligations (vs. our use of athymic rats with ischemia-reperfusion injury). While these results demonstrated a beneficial effect of poly-cell therapy, the authors did not detect stable grafts in any of the groups, indicating that the effects seen were paracrine in nature. Indeed, we are not aware of any studies in the literature that have demonstrated robust cardiomyocyte and supportive cell type engraftment in the long term following myocardial infarction. In contrast, our grafts, both cardiac as well as epicardial, and related functional benefits were

detectable up to three months post transplantation, providing evidence for longevity and potential perpetuation of benefits in the long term.

In conclusion, hESC-derived epicardial cells are a promising tool to advance regenerative cardiovascular medicine, including cell transplantation as well as tissue engineering strategies. Future studies are warranted to better understand the mechanisms through which epicardial cells propagate the observed benefits and investigate their function in models that more closely match clinical application.

Online Methods

Preparation of hESC-derived epicardial cells and hESC-derived cardiomyocytes

Epicardial cells were differentiated from GFP-transgenic hESCs as previously described[1]. Briefly, hESCs (H9, WiCell, Madison) were maintained in a chemically defined medium (CDM-BSA) containing Activin-A (10 ng/ml, R&D Systems) and FGF2 (12 ng/ml, R&D Systems). Chemically defined medium consisted of IMDM (250 ml, Life Technologies), Ham's F12 (250 ml, Life Technologies), Pen/Strep (5 ml, Life Technologies), Insulin (350 µl, Roche), Transferrin (250 µl, Roche), chemically defined 100x lipid concentrate (5 ml, Life Technologies) and monothioglycerol (20 µl, Sigma). Differentiation to lateral mesoderm was performed as previously described in CDM-PVA, containing polyvinyl alcohol (PVA, 1 mg/ml, Sigma)[2]. In brief, early mesoderm differentiation was started with a combination of CDM-PVA, FGF2 (20 ng/ml), LY294002 (10 µM, Sigma) and BMP4 (10 ng/ml, R&D) for 1.5 days. Then, lateral mesoderm differentiation was started in CDM-PVA, FGF2 (20 ng/ml) and BMP4 (50 ng/ml) for 3.5 days. To induce epicardial differentiation, cells were resuspended as single cells in CDM-PVA, WNT3A (25ng/ml, R&D), BMP4 (50ng/ml) and RA (4µM, Sigma) at a seeding density of $2.5\times10^4/cm^2$ for 10 days and the medium was changed half way through the differentiation. To generate epicardium-derived fibroblasts, epicardial cells were re-plated as single cells at a seeding density of $2.5\times10^4/cm^2$ and were grown under the influence of VEGF-B (50 ng/ml, Peprotech) and FGF2 (50 ng/ml) for 12 days. Flow cytometry was performed on day 10 epicardial cells using TCF21 (Atlas antibodies, HPA013189) and WT1 (Abcam, Ab89910) antibodies on BD FACS Calibur (BD Bioscience) analysed using FlowJo VX software version 9.9.4 (Fig. 1, panel b, Supplementary Fig. 8 and 19).

For derivation of mesenchymal stem cells from hESCs, colonies were passaged, resuspended in CDM-PVA containing FGF2 (12 ng/ml) and SB (10µM) and seeded at a density of 30 colonies/cm^2 on gel-MEF coated plates. Cells were enzymatically dispersed and passaged 4 times in CDM-PVA, containing FGF and SB before being split one more time in DMEM-F12 containing 10% fetal bovine serum for long-term maintenance. Primary mesenchymal stem cells (gift from Osiris) were also maintained in DMEM-F12 containing 10% fetal bovine serum.

Cardiomyocytes were generated from hESCs with the ABCX method as previously described[3, 4]. In brief, hESCs (RUES2, Female line, Rockefeller University, NIH registry number 0013) were maintained in feeder-free irradiated mouse embryonic fibroblast (iMEF)-conditioned media containing bFGF (4ng/ml, Peprotech). Cells were seeded as

single cells ($1\times10^5/cm^2$) on matrigel (BD) coated plates with conditioned media including Chiron 99021 (1μM, Cayman Chemical) and ROCK inhibitor (Y-27632). The following day (day 0), the media was aspirated and cells were fed with RPMI media supplemented with B27 (Invitrogen) containing Activin A (100ng/ml) for 18 hours. On day 1, media was aspirated and cells were fed with RPMI media plus B27 containing BMP4 (5ng/ml) and Chiron 99021 (1μM) for 48 hours. On day 3, media was aspirated and replaced with RPMI media plus B27 containing Xav 939 (1μM, Torcis). On day 5, the medium was replaced with RPMI media plus B27. On day 7, the media was replaced with RPMI containing B27 with insulin (Invitrogen) and was consequently replaced every other day until termination of the protocol.

Cardiomyocytes were frozen down on day 21 and the same batch was used for the entirety of the study. Flow cytometry was performed on thawed cells using cTnT antibody (Thermo, MS-295-P) on BD FACSCanto II (Beckton Dickinson, San Jose, CA) and analysed using FACSDiva software (BD Biosciences), revealing a purity of 97.1%±0.5 (cTnT+, Fig. 1, panel b).

Epicardial cells were heat-shocked on the day prior to cell transplantation, cardiomyocytes prior to freezing, both for 30 minutes at 42.5°. On the day of cell transplantation, epicardial cells and cardiomyocytes were enzymatically dispersed, counted and resuspended in 100μl volume per rat of matrigel and prosurvival cocktail (PSC). PSC consisted of 50% (vol/vol) Matrigel and ZVAD-FMK (100μM, Calbiochem), Bcl-XL (50nM, Calbiochem), Cyclosporin A (200 nM, Wako Pure Chemicals), Pinacidil (50μ, Sigma) and IGF-1 (100ng/ml, Peprotech). Cell preparations either contained Matrigel plus PSC as vehicle controls or 5×10^6 epicardial cells or 10×10^6 cardiomyocytes or the combination of 5×10^6 epicardial cells and 10×10^6 cardiomyocytes in matrigel/PSC.

Mycoplasma screening was performed on all cells on a regular basis and found to be negative.

Generation and functional assessment of 3D-EHT

In order to cast the tissue constructs, wells were fabricated using polydimethylsiloxane (PDMS) (PDMS, Sylgard 184; Dow Corning, Midland, MI). PDMS linker and base were mixed in a 1:10 mass-ratio and poured in laser-etched acrylic negative templates featuring 4 wells measuring 3×8×2 mm and containing a 1 mm diameter post positioned at 1.5mm from each end. The PDMS was baked at 65°C overnight, removed from the negatives, and then autoclaved. Prior to casting the tissues, the PDMS wells were treated with 5% pluronic acid F127 solution (Sigma, P2443) for 1 hour.

Cardiomyocytes used for construct studies were frozen down on day 21 of the differentiation and given 5 days in culture to recover. During construct casting, cardiomyocytes and epicardial cells were trypsinized and mixed in a collagen gel containing 10x RPMI-1640 medium (Sigma), NaOH, geltrex (Invitrogen, A1413202), collagen I Rat Protein (Gibco Life Technologies, A1048301) and water. The cell-gel solution was poured into the PDMS wells and allowed to solidify for 30 minutes at 37°C. Each construct contained either 5×10^5 cardiomyocytes alone or 5×10^5 cardiomyocytes plus 5×10^4 supportive cells. Constructs

were then fed with 7ml of RPMI media plus B27 plus insulin every other day, and spontaneous contractions were observed within 7 days. All constructs were cultured for 14 days, fixed with 4% paraformaldehyde, treated with 30% sucrose at 4°C overnight and finally cryoembedded and sectioned.

Myofibril alignment was quantified using an orientation correlation function (OCF) as previously described[5]. OCF = 0.5 (cos (2θ) + 1), where θ is the difference between the angle of the myofibril fibril and the longitudinal cardiomyocyte axis.

For assessment of Ca^{2+}-handling 14 day-old constructs were incubated with fluo-4, AM (Invitrogen, Molecular Probes) for 20 minutes at 37°C. Videos were taken with a Sony Handycam (Vixia HFS20) attached on a fluorescent microscope (Nikon Eclipse TS100). Videos were subsequently converted to frames, imported and analysed using Image J software, normalising the Ca^{2+}-signal to baseline.

Force measurement of constructs was performed after 2 weeks in culture as previously described[6]. In brief, constructs were removed from the PDMS wells and suspended between a force transducer (Aurora Scientific, model 400A) and length controller (Aurora Scientific, model 312B). To assess the Frank-Starling relationship, constructs were stretched from their resting length to an additional 25% strain in 6 steps while being bathed in a HEPES-buffered Tyrode solution held at 37°C. Force traces were first recorded without electrical stimulation and subsequently with 1, 1.5, 2 and 3 Hz at 5V and 50ms pulse duration. Passive tension and active force traces were recorded and analysed using customized LabView and MATLAB software. A total of 9 independent constructs were generated for each group and used for morphometric and functional analysis. The only exclusion criterion was tissue damage of the integrity of the loop regions. Cardiomyocytes were used from one frozen batch to ensure constant ultra-high purity and epicardial cells were used from three different differentiations.

Gene expression analysis

EHTs were dissociated and gene expression analyses performed after 2 weeks in culture. Total cellular RNA was extracted with ARCTURUS® PicoPure® RNA Isolation Kit (Applied Biosystems, KIT0103) with the following modifications. EHTs were placed in Lysing Matrix D beads (MP Biomedicals, 116913050) and 200µl Extraction Buffer and homogenized using a FastPrep-24™ 5G Instrument (MP Biomedicals). The resulting lysate was transferred to a fresh tube and incubated at 42°C for 30min. 70% ethanol was added to the RNA lysate and loaded into a pre-conditioned column. All subsequent steps were performed according to the supplier's recommendations, including DNase I treatment. 10µl of eluted RNA (corresponding to 100–150ng) were subjected to reverse transcription using Maxima First Strand kit (Thermo, K1641) according to the manufacturer's protocol. Quantitative real-time reverse transcription PCR (RT-qPCR) was performed with Fast SYBR Green Master Mix (Thermo, 4385610) using 5ng of cDNA and 100nM forward and reverse primers. Reactions were run on a 7900HT Fast Real-Time PCR System (Applied Biosystem, 4329001), and data was analyzed using the ΔΔCt method using HPRT1 as the housekeeping gene. Primers were designed using PrimerBlast and confirmed to amplify a single product. A complete list is provided in Supplementary table 3.

Injection of hPSC-derived epicardial cells in chicken embryos

Chicken (*Gallus gallus domesticus*) eggs (Winter Egg Farm, Cambridge, UK) were incubated in a digital cabinet incubator (OVA Easy 380, Brinsea) at 38 degrees. At Hamburger Hamilton developmental stage 19 (HH19), the eggshell was fenestrated, the window covered with parafilm (VWR) and eggs were placed horizontally in the incubator. At HH35, epicardial cells were transplanted in PSC with matrigel (1:2 dilution) onto the chorionic chicken vasculature. HESCs were fully differentiated to epicardial cells before administration into the chicken embryos. The eggs were then returned in the incubator until stage HH40. The matrigel plugs were harvested and fixed in 4% paraformaldehyde before being stained with anti-HLA1 (abcam) anti-SM22alpha (Abcam) and sambucus nigra lectin (Vector laboratories).

Myocardial infarction and cell transplantation

All studies were approved by the University of Washington Animal Care and Use Committee (IACUC; protocol number 2225–04) and were conducted in accordance with US NIH Policy on Humane Care and Use of Laboratory Animals. The study design comprised two feasibility studies and one definitive study. The first study was designed to assess the acute survival and fate of hESC-EPI. Animals either received 2×10^6 (n=4) or 4×10^6 (n=4) epicardial cells or a vehicle control injection (n=4). In a second feasibility study, designed to assess long term survival of epicardial cells and their function animals randomly received either a 6×10^6 epicardial cells (n=6) or a vehicle control injection (n=4). The definitive study was conducted to assess the trophic effect of the epicardium on cardiomyocytes. The definitive study design comprised the following four study arms: 5×10^6 epicardial cells (n=15), 10×10^6 cardiomyocytes (n=14), 5×10^6 epicardial cells plus 10×10^6 cardiomyocytes (n=14) or vehicle control (n=13). Animal deaths and cellular engraftment is presented in supplementary table 4.

The protocol for cell implantation has been previously detailed[7, 8]. In brief, male athymic Sprague Daley rats (Harlan/Envigo) underwent anaesthesia through intraperitoneal injection of 68.2 mg/kg Ketamine and 4.4 mg/kg Xylazine, intubated and mechanically ventilated with room air and supplemented oxygen. A second dose of Ketamine and Xylazine was administered 20 minutes later. Animals were placed on a heating pad connected with a rectal temperature probe, which ensured maintenance of body temperature at 37°C. A thoracotomy was subsequently performed, the anterior surface of the heart was exposed and the left anterior descending (LAD) coronary artery was visualized. The LAD was consequently ligated for 60 minutes after which the ligation was removed, the animals reperfused and the chest aseptically closed. Four days post myocardial infarction animals were anesthetized with Isoflurane before undergoing a second thoracotomy for intramyocardial cell transplantations. Animals were subsequently randomly assigned to one of the treatment groups and cells were injected into the infarct zone. The chest was subsequently closed and the animals were postoperatively monitored.

To optimize graft retention animals received a subcutaneous injection of 5 mg/kg Cyclosporine A on the day before surgery until 7 days after the surgery. To assess cell proliferation in the cell grafts animals were injected with of 50 mg/kg BrdU on days 1 4, 7,

and 14 post cell injection. The cohort of animals that was followed up for three months additionally received one BrdU injection 24 hours before the termination of the study.

Echocardiography

All animals underwent echocardiographic exams at baseline before myocardial infarction, 4 days after the infarct and 28 days after cell transplantation. A subset of animals were maintained and imaged at 84 days post-transplantation. Briefly, animals were lightly anesthetized with inhaled isoflurane (Novaplus) and scanned by transthoracic echocardiography (GE Vivid 7) using a 10S (10MHz) paediatric probe. The endpoints acquired comprised fractional shortening (%), left-ventricular diastolic dimension (LVEDD) and left-ventricular systolic dimension (LVESD). LVDD and LVESD are expressed in millimetres (mm). The images were anonymised and a primary reader made measurements in a blinded manner. For validation purposes an independent investigator analysed a sample set of images in a blinded fashion prior to analysis of the entire dataset and at the end to ensure consistency in measurements. The respective Bland-Altman plots and Intra Class Correlation Coefficients of these two tests are presented in Supplementary Figure 20. Details of histologic and echocardiographic parameters are presented in Supplementary table 1.

Immunocytochemistry and Immunohistochemistry

For immunocytochemistry, cells were fixed in 4% paraformaldehyde, permeabilized with 0.5% Triton X-100 in phosphate-buffered saline (PBS) and blocked in 3% BSA/PBS for 45 minutes at room temperature. Primary antibody incubations were performed at 4°C overnight. The next day, cells were washed and incubated with Alexa-Fluor conjugated secondary antibodies for 45 minutes at room temperature (RT) before staining with 49,6-diamidino-2-phenylindole (DAPI) for 10 minutes to visualize the nuclei. For immunohistochemistry (IHC), hearts were excised post mortem and prepared as described[8]. Briefly, hearts were washed in PBS, kept in saturated KCl for 20 minutes and subsequently fixed in 4% paraformaldehyde and were paraffin sectioned (5 mm). For IHC stainings, slides were deparafinized, underwent heat-mediated antigen retrieval for 15 minutes and blocked with 5% BSA/PBS containing 0.3% Triton X-100 for one hour at RT, followed by incubation with primary antibodies at 4°C overnight and fluorescent secondary antibodies were applied at room temperature for 60 minutes on the consecutive day. All antibodies used for immunocytochemistry and immunohistochemistry studies are detailed in Supplementary table 5.

For quantification of sarcomeric length, a total number of 1271 sarcomeres (129 cardiomyocytes) were quantified *in vitro* (9 constructs) and 4660 sarcomeres (407 cardiomyocytes) were quantified *in vivo* (37 animals) by manual measurements in a blinded fashion.

Infarct and graft quantification

To assess infarct size, slides were stained with picrosirius red/ fast-green stain. Subsequently in the infarcted sections, picrosirius red positive area was quantified and normalized to the left ventricular area in each section. For quantification of cardiac graft size, slides were stained overnight with human mitochondria antibody (Novus) and α-Actinin (Abcam) to

quantify the size of the human cardiac grafts followed by 1 hour incubation with Alexa Fluor-488 donkey anti-rabbit and Alexa Fluor-568 goat anti-mouse secondary antibodies (Invitrogen). The corresponding graft size was then normalized to the size of the infarct area. All animals were used for analysis except one animal in the CM only study arm, which didn't exhibit a detectable graft. Images were acquired on a Nikon TiE Inverted Widefield Fluorescence High-Resolution Microscope. To assess epicardial grafts, anti-GFP (Novus) and anti-human Mitochondria (Novus) antibodies were used. For investigation of epithelial to mesenchymal transition of grafted epicardial cells, slides were stained with antibodies directed against GFP (Novus), Vimentin (Dako) and Wide-spectrum Cytokeratin (Dako). To determine the fate of epicardial cells, slides were co-stained with antibodies directed against human Mitochondria (Novus) and cardiomyocyte (alpha-Actinin (Abcam)), endothelial cells (human Lectin (Ulex europaeus, Vector)), smooth muscle cells, (Smooth Muscle α-Actin (Dako)), or fibroblasts (S100A4 (Abcam)). To detect cardiac grafts, antibodies directed either against human mitochondria and α-Actinin or against β-MHC (Developmental Studies Hybridoma Bank) were used. For assessment of microvascular density, slides were stained with CD31/PECAM (Novus) and either β-MHC (Developmental Studies Hybridoma Bank) or cTnI (Abcam). For quantification of microvascular density in cardiac grafts, the infarct zone and the non-injured border zone, 9 high power images were taken in each of the three areas of interest. The number of lumen was counted and expressed as vessel number/area (mm^2). All images were acquired in technical replicates per animal on a Zeiss LSM700 microscope using ZEN software and were subsequently analysed using Image J software. A detailed description of the antibodies and dilutions is provided in supplemental online table 1.

RNA-sequencing

The starting material for RNA sequencing was hESC-derived epicardium as used for all *in vitro* and *in vivo* experiments. For bulk RNA-sequencing total RNA was extracted with the RNeasy Mini kit according to the manufacturer's instructions (Qiagen). This was followed by RNAse treatment to remove contaminating DNA. Samples were consecutively sent to the Genomics facility at the Wellcome Trust - Medical Research Council Cambridge Stem Cell Institute, where cDNA libraries were generated using the SMARTer Stranded Total RNA-Seq Kit.

All samples were sequenced on two lanes of Illumina HiSeq2500. Short reads were mapped to the *Homo Sapiens* genome GRCh38 using HISAT2[9]. For each sample, the bam files corresponding to both lanes were merged with bamtools[10]. This data has been deposited in NCBI's Gene Expression Omnibus (Edgar et al., 2002) and are accessible through GEO Series accession number GSE122714 (https://www.ncbi.nlm.nih.gov/geo/query/acc.cgi?acc=GSE122714)[11].

The number of reads per sample vary from 10 millions (NC1) to 24 millions (NC2). Quality control and read count was performed with SeqMonk (https://www.bioinformatics.babraham.ac.uk/projects/seqmonk/). Differential Expression analysis between differentiated epicardium and NC cells was performed with DESeq2[12]. The list of 8261 differentially expressed genes was filtered to retain: 1) only genes encoding putatively

secreted proteins, according to the Human Protein Atlas (http://www.proteinatlas.org/humanproteome/secretome,[9]). 2) only genes annotated with the gene ontology term "extracellular matrix organisation" using QuckGO (https://www.ebi.ac.uk/QuickGO,[13]). The heatmap only displays differentially expressed genes with an adjusted p-value < 1e-7. It was performed using the function heatplot of the package made4 on the log2 of reads per million reads values[14]. For clustering, heatplot uses Pearson correlation distances and the average agglomeration method. The GO enrichment was performed with WebGestalt[15]. A complete list of the genes and their expression is shown in supplementary table 2.

Statistics

All *in vitro* studies were performed as three biological replicates (independent experiments performed on different days), each of which was performed using 3 technical replicates. All *in vivo* data specifically state the number of animals assessed for each time point. The normal distribution of our values was confirmed using the D'Agostino & Pearson omnibus normality test where appropriate. Variance between samples was tested with the Brown-Forsythe test. Statistical testing was performed using an unpaired t-test for two group comparisons and a paired t-test for comparison of two paired groups. For multiple-group comparison a one-way ANOVA with a post-hoc Tukey test was used if the group variance was equal and a Kruskall-Wallis test with Dunn's correction for multiple comparisons was applied for groups with unequal variance. Measuring two-sided significance, a p-value of 0.05 was considered statistically significant. All analysis was performed using GraphPad Prism software in a blinded fashion. All results are expressed as mean± SD., unless otherwise stated.

For all *in vivo* experiments group sizes were estimated based on power analyses using previous study variance. While no formal methods of randomization were used, the animals were randomly selected by a technician who was blinded to treatment. Analysis of all histology slides as well as all functional data were analysed in a blinded fashion. Death was the only exclusion criteria for further histologic and functional analysis. Supplementary table 4 details animal mortality and grafting.

Further details can be found in the Life Sciences Reporting Summary.

Supplementary Material

Refer to Web version on PubMed Central for supplementary material.

Acknowledgements

This work was supported by the British Heart Foundation (BHF; Grants NH/11/1/28922, G1000847, FS/13/29/30024 and FS/18/46/33663), Oxford-Cambridge Centre for Regenerative Medicine (RM/13/3/30159), the UK Medical Research Council (MRC) and the Cambridge Hospitals National Institute for Health Research Biomedical Research Centre funding (SS), as well as National Institutes of Health Grants P01HL094374, P01GM081619, R01HL128362 and a grant from the Fondation Leducq Transatlantic Network of Excellence (CEM).

J.B. was supported by a Cambridge National Institute for Health Research Biomedical Research Centre Cardiovascular Clinical Research Fellowship and subsequently, by a BHF Studentship (Grant FS/13/65/30441). DI received a University of Cambridge Commonwealth Scholarship. LG is supported by BHF Award RM/l3/3/30159 and LPO is funded by a Wellcome Trust Fellowship (203568/Z/16/Z). NF was supported by BHF grant RG/13/14/30314. NL was supported by the Biotechnology and Biological Sciences Research Council (Institute

Strategic Programmes BBS/E/B/000C0419 and BBS/E/B/000C0434). SS and MB were supported by the British Heart Foundation Centre for Cardiovascular Research Excellence. Core support was provided by the Wellcome-MRC Cambridge Stem Cell Institute (203151/Z/16/Z), The authors thank Osiris for provision of the primary mesenchymal stem cells [47].

Competing financial interest: A patent has been filed on the cardiac application of epicardial cells, on which CEM, SS and JB are co-inventors (WO2018170280A1). CEM is a scientific founder and equity holder in Cytocardia.

References

1. Braunwald E Shattuck lecture--cardiovascular medicine at the turn of the millennium: triumphs, concerns, and opportunities. N Engl J Med. 1997;337(19):1360–9. [PubMed: 9358131]
2. Mozaffarian D, Benjamin EJ, Go AS, Arnett DK, Blaha MJ, Cushman M, et al. Heart Disease and Stroke Statistics-2016 Update: A Report From the American Heart Association. Circulation. 2016;133(4):e38–360. [PubMed: 26673558]
3. McMurray JJ, Petrie MC, Murdoch DR, Davie AP. Clinical epidemiology of heart failure: public and private health burden. European heart journal. 1998;19 Suppl P:P9–16. [PubMed: 9886707]
4. Bertero A, Murry CE. Hallmarks of cardiac regeneration. Nature reviews Cardiology. 2018;15(10): 579–80.
5. Weinberger F, Mannhardt I, Eschenhagen T. Engineering Cardiac Muscle Tissue: A Maturating Field of Research. Circulation research. 2017;120(9):1487–500. [PubMed: 28450366]
6. Burridge PW, Matsa E, Shukla P, Lin ZC, Churko JM, Ebert AD, et al. Chemically defined generation of human cardiomyocytes. Nature methods. 2014;11(8):855–60. [PubMed: 24930130]
7. Lian X, Hsiao C, Wilson G, Zhu K, Hazeltine LB, Azarin SM, et al. Robust cardiomyocyte differentiation from human pluripotent stem cells via temporal modulation of canonical Wnt signaling. Proceedings of the National Academy of Sciences of the United States of America. 2012;109(27):E1848–57. [PubMed: 22645348]
8. Laflamme MA, Chen KY, Naumova AV, Muskheli V, Fugate JA, Dupras SK, et al. Cardiomyocytes derived from human embryonic stem cells in pro-survival factors enhance function of infarcted rat hearts. Nature biotechnology. 2007;25(9):1015–24.
9. Patsch C, Challet-Meylan L, Thoma EC, Urich E, Heckel T, O'Sullivan JF, et al. Generation of vascular endothelial and smooth muscle cells from human pluripotent stem cells. Nature cell biology. 2015;17(8):994–1003. [PubMed: 26214132]
10. Orlova VV, van den Hil FE, Petrus-Reurer S, Drabsch Y, Ten Dijke P, Mummery CL. Generation, expansion and functional analysis of endothelial cells and pericytes derived from human pluripotent stem cells. Nature protocols. 2014;9(6):1514–31. [PubMed: 24874816]
11. Cheung C, Bernardo AS, Trotter MW, Pedersen RA, Sinha S. Generation of human vascular smooth muscle subtypes provides insight into embryological origin-dependent disease susceptibility. Nature biotechnology. 2012;30(2):165–73.
12. Iyer D, Gambardella L, Bernard WG, Serrano F, Mascetti VL, Pedersen RA, et al. Robust derivation of epicardium and its differentiated smooth muscle cell progeny from human pluripotent stem cells. Development (Cambridge, England). 2015;142(8):1528–41.
13. Witty AD, Mihic A, Tam RY, Fisher SA, Mikryukov A, Shoichet MS, et al. Generation of the epicardial lineage from human pluripotent stem cells. Nature biotechnology. 2014;32(10):1026–35.
14. Palpant NJ, Pabon L, Roberts M, Hadland B, Jones D, Jones C, et al. Inhibition of beta-catenin signaling respecifies anterior-like endothelium into beating human cardiomyocytes. Development (Cambridge, England). 2015;142(18):3198–209.
15. Palpant NJ, Pabon L, Friedman CE, Roberts M, Hadland B, Zaunbrecher RJ, et al. Generating high-purity cardiac and endothelial derivatives from patterned mesoderm using human pluripotent stem cells. Nature protocols. 2017;12(1):15–31. [PubMed: 27906170]
16. Shiba Y, Fernandes S, Zhu WZ, Filice D, Muskheli V, Kim J, et al. Human ES-cell-derived cardiomyocytes electrically couple and suppress arrhythmias in injured hearts. Nature. 2012;489(7415):322–5. [PubMed: 22864415]

17. Weinberger F, Breckwoldt K, Pecha S, Kelly A, Geertz B, Starbatty J, et al. Cardiac repair in guinea pigs with human engineered heart tissue from induced pluripotent stem cells. Science translational medicine. 2016;8(363):363ra148.
18. Chong JJ, Yang X, Don CW, Minami E, Liu YW, Weyers JJ, et al. Human embryonic-stem-cell-derived cardiomyocytes regenerate non-human primate hearts. Nature. 2014.
19. Shiba Y, Gomibuchi T, Seto T, Wada Y, Ichimura H, Tanaka Y, et al. Allogeneic transplantation of iPS cell-derived cardiomyocytes regenerates primate hearts. Nature. 2016;538(7625):388–91. [PubMed: 27723741]
20. Liu YW, Chen B, Yang X, Fugate JA, Kalucki FA, Futakuchi-Tsuchida A, et al. Human embryonic stem cell-derived cardiomyocytes restore function in infarcted hearts of non-human primates. Nature biotechnology. 2018;36(7):597–605.
21. van den Berg CW, Okawa S, Chuva de Sousa Lopes SM, van Iperen L, Passier R, Braam SR, et al. Transcriptome of human foetal heart compared with cardiomyocytes from pluripotent stem cells. Development (Cambridge, England). 2015;142(18):3231–8.
22. Guadix JA, Carmona R, Munoz-Chapuli R, Perez-Pomares JM. In vivo and in vitro analysis of the vasculogenic potential of avian proepicardial and epicardial cells. Developmental dynamics : an official publication of the American Association of Anatomists. 2006;235(4):1014–26. [PubMed: 16456846]
23. Gittenberger-de Groot AC, Vrancken Peeters MP, Mentink MM, Gourdie RG, Poelmann RE. Epicardium-derived cells contribute a novel population to the myocardial wall and the atrioventricular cushions. Circulation research. 1998;82(10):1043–52. [PubMed: 9622157]
24. Dettman RW, Denetclaw W Jr., Ordahl CP, Bristow J. Common epicardial origin of coronary vascular smooth muscle, perivascular fibroblasts, and intermyocardial fibroblasts in the avian heart. Dev Biol. 1998;193(2):169–81. [PubMed: 9473322]
25. Manner J Does the subepicardial mesenchyme contribute myocardioblasts to the myocardium of the chick embryo heart? A quail-chick chimera study tracing the fate of the epicardial primordium. Anat Rec. 1999;255(2):212–26. [PubMed: 10359522]
26. Ieda M, Tsuchihashi T, Ivey KN, Ross RS, Hong TT, Shaw RM, et al. Cardiac fibroblasts regulate myocardial proliferation through beta1 integrin signaling. Dev Cell. 2009;16(2):233–44. [PubMed: 19217425]
27. Eid H, Larson DM, Springhorn JP, Attawia MA, Nayak RC, Smith TW, et al. Role of epicardial mesothelial cells in the modification of phenotype and function of adult rat ventricular myocytes in primary coculture. Circulation research. 1992;71(1):40–50. [PubMed: 1606667]
28. Stuckmann I, Evans S, Lassar AB. Erythropoietin and retinoic acid, secreted from the epicardium, are required for cardiac myocyte proliferation. Dev Biol. 2003;255(2):334–49. [PubMed: 12648494]
29. Weeke-Klimp A, Bax NA, Bellu AR, Winter EM, Vrolijk J, Plantinga J, et al. Epicardium-derived cells enhance proliferation, cellular maturation and alignment of cardiomyocytes. Journal of molecular and cellular cardiology. 2010;49(4):606–16. [PubMed: 20655924]
30. Braitsch CM, Kanisicak O, van Berlo JH, Molkentin JD, Yutzey KE. Differential expression of embryonic epicardial progenitor markers and localization of cardiac fibrosis in adult ischemic injury and hypertensive heart disease. Journal of molecular and cellular cardiology. 2013;65:10.1016/j.yjmcc.2013.10.005.
31. Ruan JL, Tulloch NL, Razumova MV, Saiget M, Muskheli V, Pabon L, et al. Mechanical Stress Conditioning and Electrical Stimulation Promote Contractility and Force Maturation of Induced Pluripotent Stem Cell-Derived Human Cardiac Tissue. Circulation. 2016;134(20):1557–67. [PubMed: 27737958]
32. Dubois NC, Craft AM, Sharma P, Elliott DA, Stanley EG, Elefanty AG, et al. SIRPA is a specific cell-surface marker for isolating cardiomyocytes derived from human pluripotent stem cells. Nature biotechnology. 2011;29(11):1011–8.
33. Winter EM, van Oorschot AA, Hogers B, van der Graaf LM, Doevendans PA, Poelmann RE, et al. A new direction for cardiac regeneration therapy: application of synergistically acting epicardium-derived cells and cardiomyocyte progenitor cells. Circulation Heart failure. 2009;2(6):643–53. [PubMed: 19919990]

34. Gerbin KA, Yang X, Murry CE, Coulombe KL. Enhanced Electrical Integration of Engineered Human Myocardium via Intramyocardial versus Epicardial Delivery in Infarcted Rat Hearts. PloS one. 2015;10(7):e0131446. [PubMed: 26161513]

35. van Tuyn J, Atsma DE, Winter EM, van der Velde-van Dijke I, Pijnappels DA, Bax NA, et al. Epicardial cells of human adults can undergo an epithelial-to-mesenchymal transition and obtain characteristics of smooth muscle cells in vitro. Stem cells (Dayton, Ohio). 2007;25(2):271–8.

36. Bax NA, Pijnappels DA, van Oorschot AA, Winter EM, de Vries AA, van Tuyn J, et al. Epithelial-to-mesenchymal transformation alters electrical conductivity of human epicardial cells. Journal of cellular and molecular medicine. 2011;15(12):2675–83. [PubMed: 21251220]

37. Kirby ML, Gale TF, Stewart DE. Neural crest cells contribute to normal aorticopulmonary septation. Science (New York, NY). 1983;220(4601):1059–61.

38. Porras D, Brown CB. Temporal-spatial ablation of neural crest in the mouse results in cardiovascular defects. Developmental dynamics : an official publication of the American Association of Anatomists. 2008;237(1):153–62. [PubMed: 18058916]

39. Jiang X, Rowitch DH, Soriano P, McMahon AP, Sucov HM. Fate of the mammalian cardiac neural crest. Development (Cambridge, England). 2000;127(8):1607–16.

40. Cai CL, Martin JC, Sun Y, Cui L, Wang L, Ouyang K, et al. A myocardial lineage derives from Tbx18 epicardial cells. Nature. 2008;454(7200):104–8. [PubMed: 18480752]

41. Gittenberger-de Groot AC, Vrancken Peeters MP, Bergwerff M, Mentink MM, Poelmann RE. Epicardial outgrowth inhibition leads to compensatory mesothelial outflow tract collar and abnormal cardiac septation and coronary formation. Circulation research. 2000;87(11):969–71. [PubMed: 11090540]

42. Ogle BM, Bursac N, Domian I, Huang NF, Menasche P, Murry CE, et al. Distilling complexity to advance cardiac tissue engineering. Sci Transl Med. 2016;8(342):342ps13.

43. Lepilina A, Coon AN, Kikuchi K, Holdway JE, Roberts RW, Burns CG, et al. A dynamic epicardial injury response supports progenitor cell activity during zebrafish heart regeneration. Cell. 2006;127(3):607–19. [PubMed: 17081981]

44. Porrello ER, Mahmoud AI, Simpson E, Hill JA, Richardson JA, Olson EN, et al. Transient regenerative potential of the neonatal mouse heart. Science. 2011;331(6020):1078–80. [PubMed: 21350179]

45. Wang J, Karra R, Dickson AL, Poss KD. Fibronectin is deposited by injury-activated epicardial cells and is necessary for zebrafish heart regeneration. Dev Biol. 2013;382(2):427–35. [PubMed: 23988577]

46. Winter EM, Grauss RW, Hogers B, van Tuyn J, van der Geest R, Lie-Venema H, et al. Preservation of left ventricular function and attenuation of remodeling after transplantation of human epicardium-derived cells into the infarcted mouse heart. Circulation. 2007;116(8):917–27. [PubMed: 17684151]

47. Pittenger MF, Mackay AM, Beck SC, Jaiswal RK, Douglas R, Mosca JD, et al. Multilineage potential of adult human mesenchymal stem cells. Science (New York, NY). 1999;284(5411):143–7.

Online references

1. Iyer D, Gambardella L, Bernard WG, Serrano F, Mascetti VL, Pedersen RA, et al. Robust derivation of epicardium and its differentiated smooth muscle cell progeny from human pluripotent stem cells. Development (Cambridge, England). 2015;142(8):1528–41.

2. Bargehr J, Low L, Cheung C, Bernard WG, Iyer D, Bennett MR, et al. Embryological Origin of Human Smooth Muscle Cells Influences Their Ability to Support Endothelial Network Formation. Stem cells translational medicine. 2016;5(7):946–59. [PubMed: 27194743]

3. Hofsteen P, Robitaille AM, Chapman DP, Moon RT, Murry CE. Quantitative proteomics identify DAB2 as a cardiac developmental regulator that inhibits WNT/beta-catenin signaling. Proceedings of the National Academy of Sciences of the United States of America. 2016;113(4):1002–7. [PubMed: 26755607]

4. Palpant NJ, Hofsteen P, Pabon L, Reinecke H, Murry CE. Cardiac development in zebrafish and human embryonic stem cells is inhibited by exposure to tobacco cigarettes and e-cigarettes. PloS one. 2015;10(5):e0126259. [PubMed: 25978043]
5. Young JL, Engler AJ. Hydrogels with time-dependent material properties enhance cardiomyocyte differentiation in vitro. Biomaterials. 2011;32(4):1002–9. [PubMed: 21071078]
6. Ruan JL, Tulloch NL, Saiget M, Paige SL, Razumova MV, Regnier M, et al. Mechanical Stress Promotes Maturation of Human Myocardium From Pluripotent Stem Cell-Derived Progenitors. Stem cells (Dayton, Ohio). 2015;33(7):2148–57.
7. Laflamme MA, Chen KY, Naumova AV, Muskheli V, Fugate JA, Dupras SK, et al. Cardiomyocytes derived from human embryonic stem cells in pro-survival factors enhance function of infarcted rat hearts. Nature biotechnology. 2007;25(9):1015–24.
8. Gerbin KA, Yang X, Murry CE, Coulombe KL. Enhanced Electrical Integration of Engineered Human Myocardium via Intramyocardial versus Epicardial Delivery in Infarcted Rat Hearts. PloS one. 2015;10(7):e0131446. [PubMed: 26161513]
9. Kim D, Langmead B, Salzberg SL. HISAT: a fast spliced aligner with low memory requirements. Nature methods. 2015;12(4):357–60. [PubMed: 25751142]
10. Barnett DW, Garrison EK, Quinlan AR, Stromberg MP, Marth GT. BamTools: a C++ API and toolkit for analyzing and managing BAM files. Bioinformatics (Oxford, England). 2011;27(12): 1691–2.
11. Edgar R, Domrachev M, Lash AE. Gene Expression Omnibus: NCBI gene expression and hybridization array data repository. Nucleic acids research. 2002;30(1):207–10. [PubMed: 11752295]
12. Love MI, Huber W, Anders S. Moderated estimation of fold change and dispersion for RNA-seq data with DESeq2. Genome biology. 2014;15(12):550. [PubMed: 25516281]
13. Binns D, Dimmer E, Huntley R, Barrell D, O'Donovan C, Apweiler R. QuickGO: a web-based tool for Gene Ontology searching. Bioinformatics (Oxford, England). 2009;25(22):3045–6.
14. Eisen MB, Spellman PT, Brown PO, Botstein D. Cluster analysis and display of genome-wide expression patterns. Proceedings of the National Academy of Sciences of the United States of America. 1998;95(25):14863–8. [PubMed: 9843981]
15. Wang J, Vasaikar S, Shi Z, Greer M, Zhang B. WebGestalt 2017: a more comprehensive, powerful, flexible and interactive gene set enrichment analysis toolkit. Nucleic acids research. 2017;45(W1):W130–w7. [PubMed: 28472511]

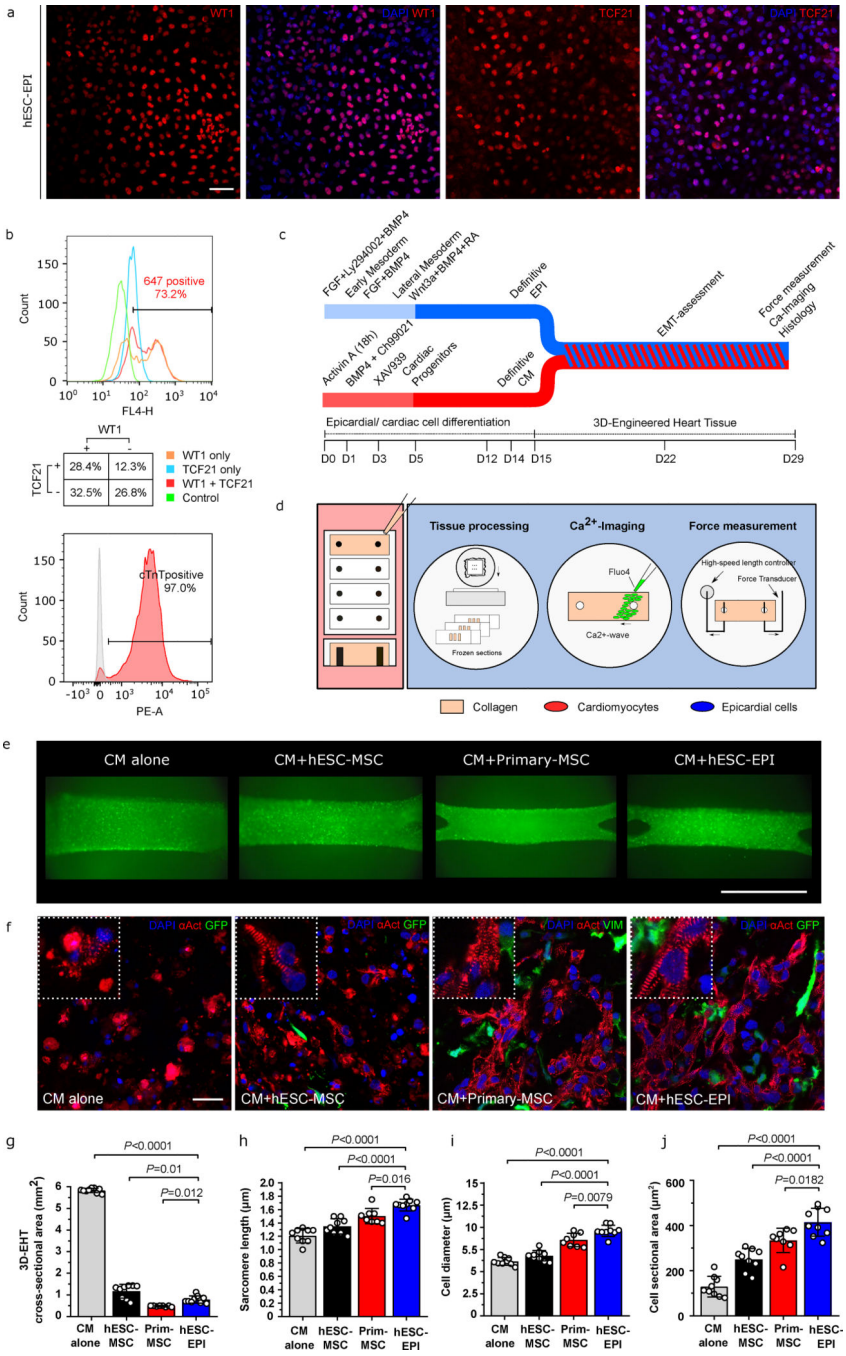

Figure 1. Generation and maturation of 3D-EHT using hESC-derived epicardial cells and cardiomyocytes.

(a) Epicardial cells derived from hESCs expressing the epicardial markers BNC1 and WT1. Scale bar: 50µm. **(b)** Purity of epicardial cells and cardiomyocytes by flow cytometry. Control groups represent secondary and isotype antibodies for epicardial cells and cardiomyocytes respectively. Flow cytometric analysis was independently repeated 3 times with similar results. **(c)** Schematic of experimental design. Epicardial cells and cardiomyocytes were derived from hESCs and co-cultured in 3D-EHT. **(d)** Schematic of 3D-

EHT using hESC-derived epicardial cells and cardiomyocytes. **(e-f)** Compaction and ultrastructure of 3D-EHT containing CM alone, CM+hESC-MSC, CM+Primary MSC or CM+hESC-EPI. Scale bars: 2.5mm and 25μm. (a, e-f) Experiments were independently repeated 9 times with similar results. **(g-j)** Quantification of tissue remodelling, sarcomeric length, cell diameter and cell sectional area.

Mean values; error bars represent SD. Two-sided *p*-values were calculated using a one-way ANOVA with post-hoc correction for multiple comparisons. CM alone, CM+hESC-MSC, CM+Primary MSC and CM+hESC-EPI, n=9, 9, 8, 9 constructs, generated independently and measured on three different days.

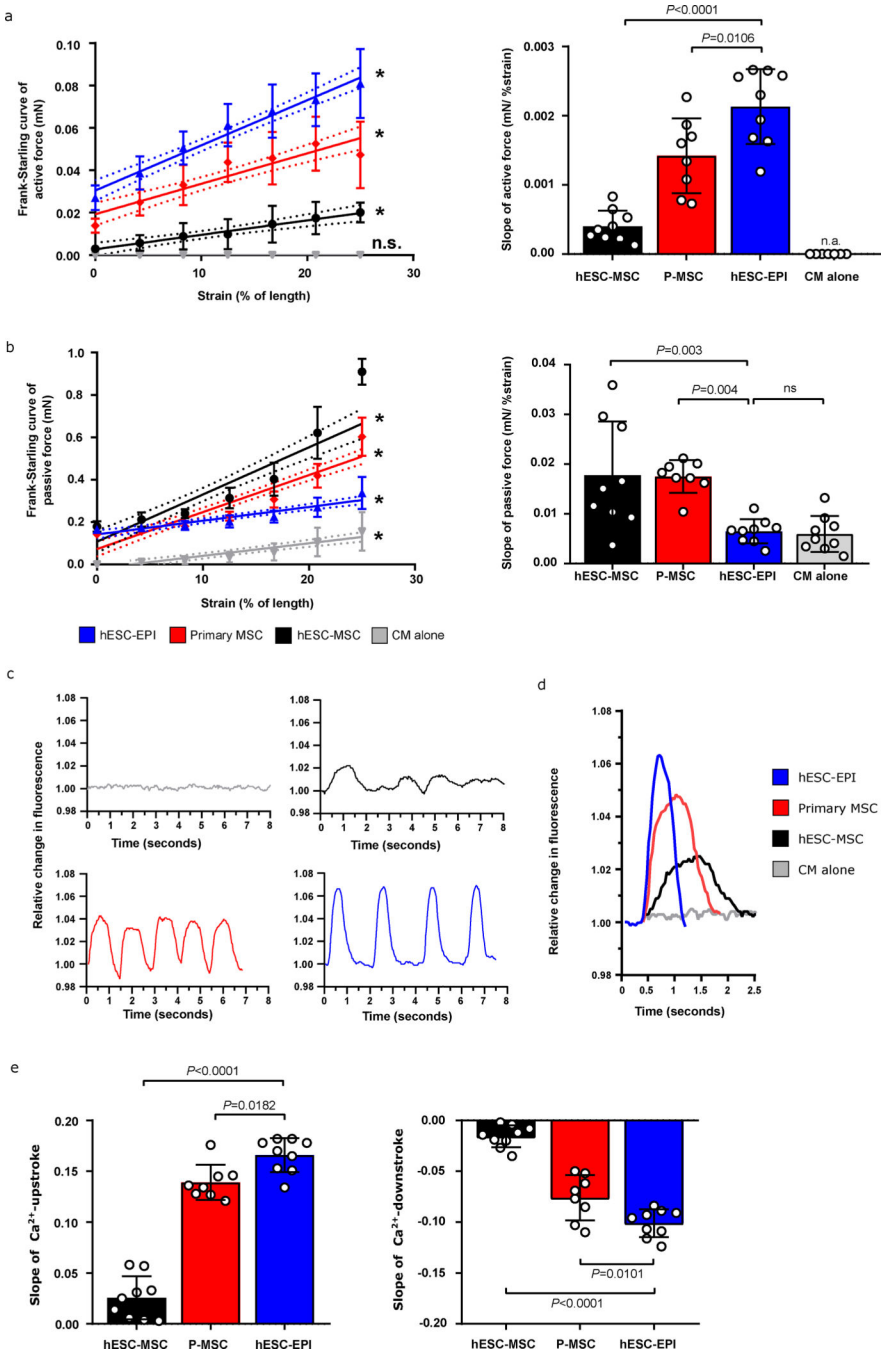

Figure 2. HESC-derived epicardial cells promote contractility and Ca^{2+}-handling of 3D-EHT.

(a) Active force generation of 3D-EHT containing CM alone, CM+hESC-MSC, CM +Primary MSC or CM+hESC-EPI. Displayed are the Frank-Starling curve of active force production and the slope of the generated curve, respectively. **(b)** Passive force of 3D-EHT containing CM alone, CM+hESC-MSC, CM+Primary MSC or CM+hESC-EPI. Displayed are the curve of passive force production and the slope of the generated curve respectively. **(c)** Representative Ca^{2+} traces of 3D-EHT. **(d)** Overlay of representative Ca^{2+} curves. **(e)** Slope of Ca^{2+}-upstroke and Ca^{2+}-downstroke. Mean values; error bars represent SD. Dotted

lines represent 95% confidence intervals. Two-sided *p*-values were calculated using a one-way ANOVA with post-hoc correction for multiple comparisons. CM alone, CM+hESC-MSC, CM+Primary MSC and CM+hESC-EPI, n=9, 9, 8, 9 constructs, generated independently and measured on three different days.

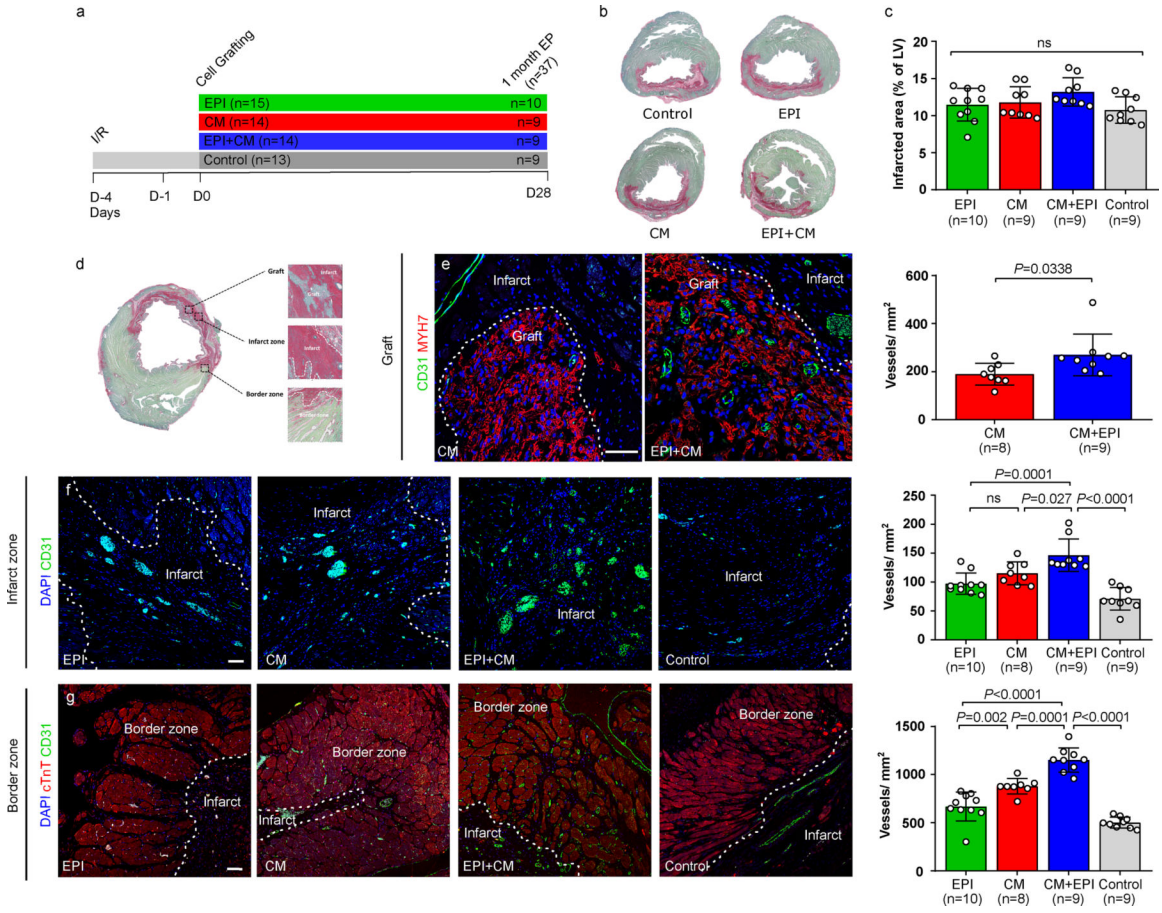

Figure 3. Co-transplantation of hESC-derived epicardial cells with cardiomyocytes promotes microvascular density.

(a) Schematic of study design. **(b)** Representative Picrosirius Red-Fast Green counterstained infarcted rat heart sections. **(c)** Quantification of myocardial infarct size. **(d)** Schematic of areas assessed for vascularisation. **(e)** Microvascular density in cardiac grafts. **(f)** Microvascular density in the infarct zone. **(g)** Microvascular density in the non-injured border zone of the infarct. Due to the presence of erythrocyte autofluorescence all quantification was performed manually to avoid erroneous detection with automated software.

Mean values; error bars represent SD. Two-sided *p*-values were calculated using a one-way ANOVA with post-hoc correction for multiple comparisons unless otherwise stated. N=36 in total for histologic analysis at the 1-month time point. Control, EPI, CM, CM+EPI, n=9, 10, 8 and 9 animals. Scale bars: 50μm.

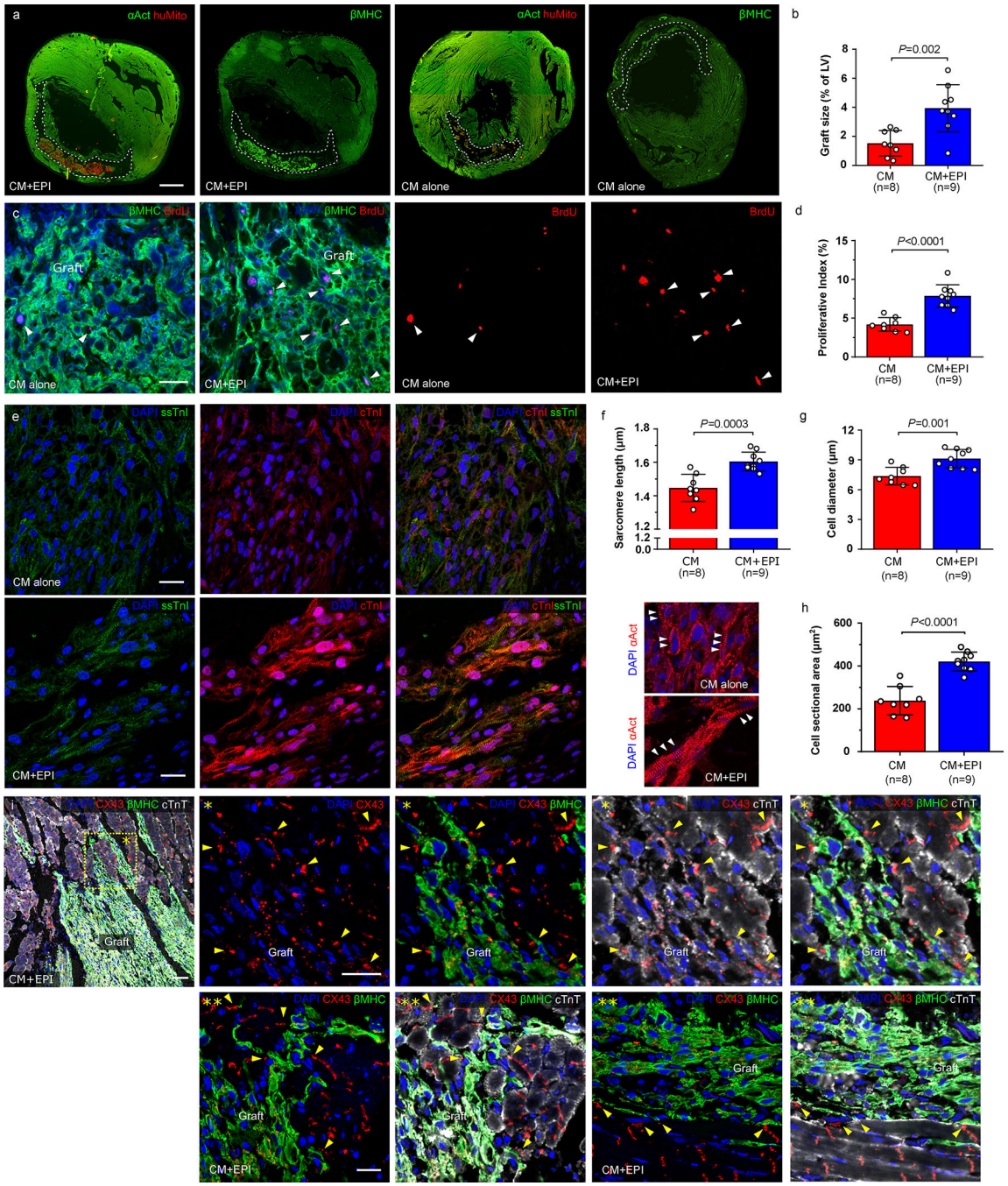

Figure 4. HESC-derived epicardial cells potentiate cardiac regeneration.

(a) Representative sections of infarcted hearts demonstrating the cardiac grafts in animals that received either hESC-derived epicardial cells and cardiomyocytes or cardiomyocytes alone. βMHC is specific for grafted human cardiomyocytes while cTnT antibody stains both rat and human cardiomyocytes. Scale bar: 2.5mm. **(b)** Quantification of cardiac graft size. **(c)** Proliferative index of human cardiomyocytes in cardiac grafts. Scale bar: 20μm. **(d)** Quantification of proliferative index. **(e)** Isoform switch of SSTnI to cTnI in cardiomyocytes *in vivo* in animals receiving EPI+CM and CM alone. Staining performed in 5 animals per

group. Scale bars: 20μm. **(f)** Quantification of sarcomeric length. **(g)** Quantification of cell diameter in cardiomyocytes *in vivo*. **(h)** Quantification of cell sectional area in cardiomyocytes *in vivo*. **(i)** Cardiac grafts and Cx43+ gap junctions with host tissue. Scale bars 50μm for (i) and 20μm for (*) and (**). (i) CX43 staining was performed on all animals. Mean values; error bars represent SD. Two-sided *p*-values were calculated using an unpaired t-test unless otherwise stated. *N*=37 in total for histologic analysis after 1 month; Control, EPI, CM, CM+EPI, *n*=9, 10, 9 and 9 animals.

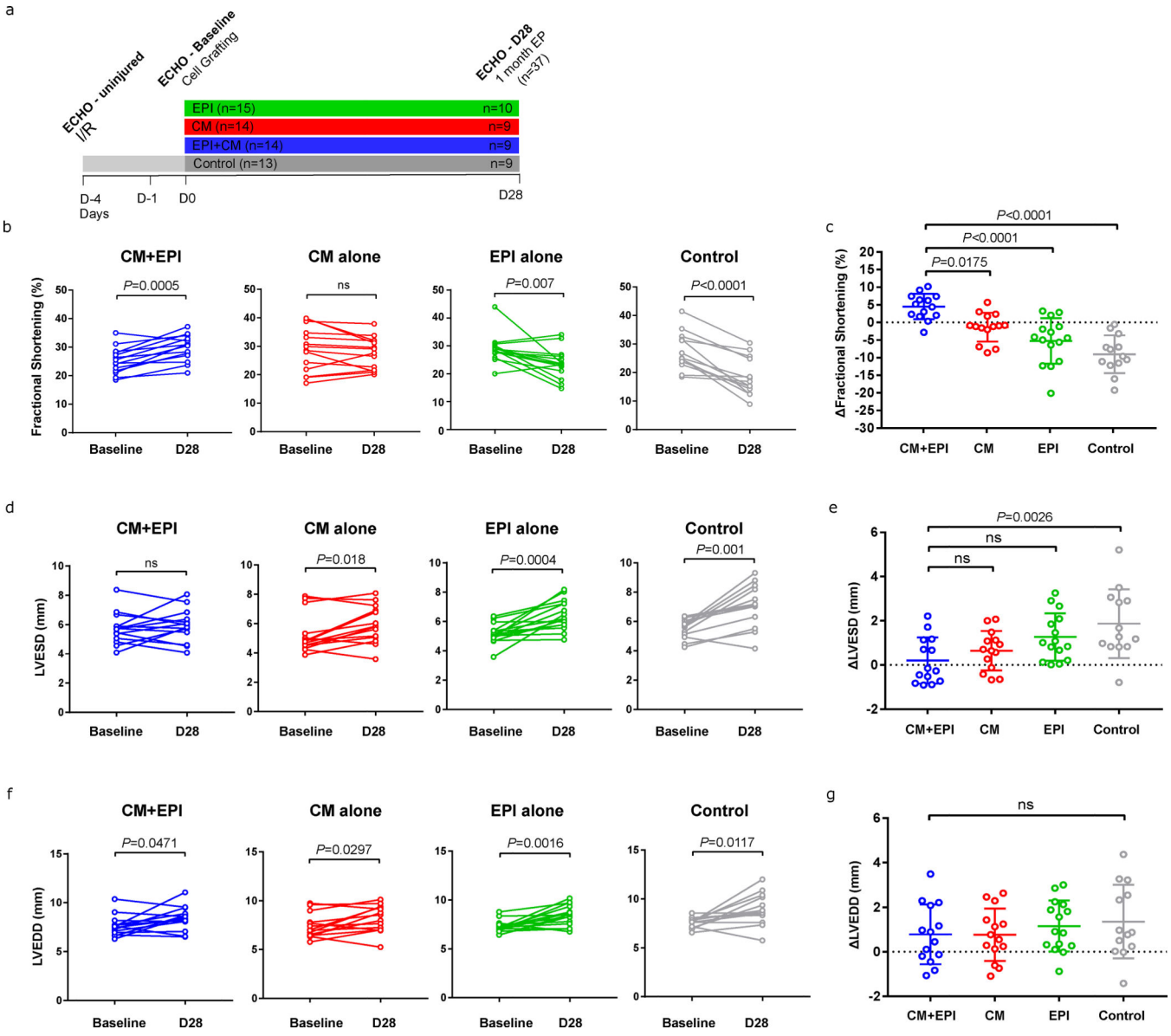

Figure 5. Co-transplantation of epicardial cells and cardiomyocytes promotes functional recovery.

(a) Schematic of study design and timing of echocardiographic data collection. **(b)** Echocardiographic effects of hESC-derived epicardial cell augmented cardiac grafts on postinfarct ventricular function. Fractional shortening values are given for the 96hr pre-treatment baseline and 1-month follow-up. **(c)** Difference in fractional shortening. **(d)** Left-ventricular end-systolic dimension (LVESD) are given for the 96hr pre-treatment baseline and 1-month follow-up. **(e)** Difference in LVEDS. **(f)** Left-ventricular end-diastolic dimension (LVEDD) are given for the 96hr pre-treatment baseline and 1-month follow-up. **(g)** Difference in LVEDD.

Mean values; error bars represent SD. Two-sided *p*-values were calculated using a paired t-test for comparison of cardiac function within groups between baseline and 1-month follow-up. If more than 2 groups were compared, a one-way ANOVA with post-hoc correction for

multiple comparisons was used. N=56 in total for functional analysis after 1 month; Control, EPI, CM, CM+EPI, n=13, 15, 14 and 14 animals.

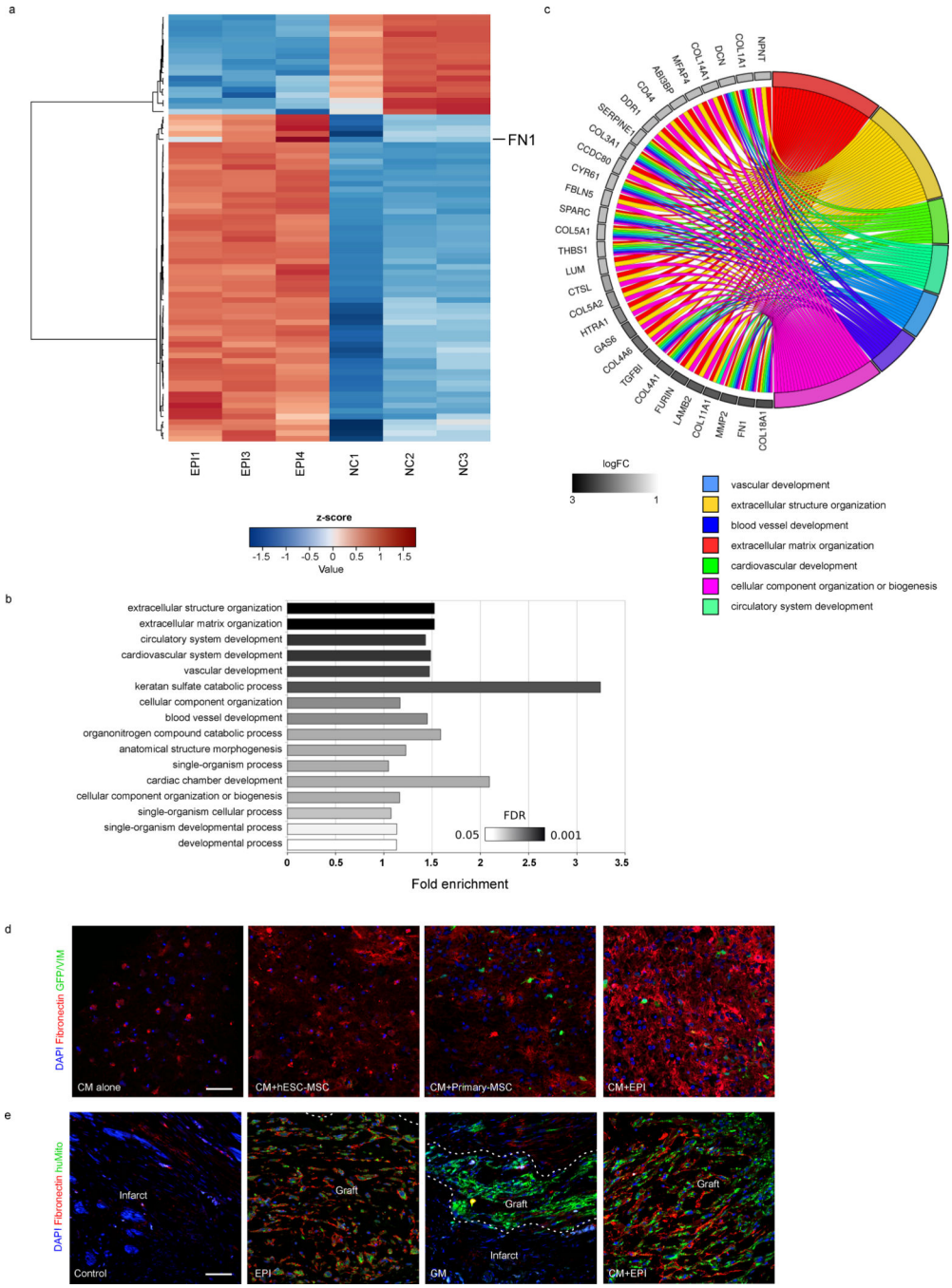

Figure 6. Epicardial secretome.

(a) Heatmap depicting differentially expressed secreted factors in epicardial cells compared to neural crest. **(b)** Gene enrichment analysis showing the top enriched GO biological processes. The 705 genes specifically enriched in the EPI secretome were subjected to a hypergeometric test against a background of the 2413 secretome genes expressed in NC or EPI. GO terms are shaded between black and white based on their false discovery rate after *Benjamini–Hochberg correction*. **(c)** Circular GO plot depicting the top GO terms enriched in EPI vs. NC associated with at least 10 genes on the right and the associated genes on the

left. Genes are shaded between black and white based on their fold enrichment in EPI compared with NC. (a-c) EPI and NC, *n*=3 and 3. **(d)** Fibronectin expression in 3D-EHT *in vitro*. CM alone, CM+hESC-MSC, CM+Primary MSC and CM+hESC-EPI, *n*=9, 9, 8, 9 constructs, generated independently and measured on different days. Scale bars 50μm. **(e)** Fibronectin expression in epicardial and cardiac grafts in animals *in vivo*. Scale bars 50μm. This staining was performed on all animals at the 1-month time point (*n*=37).